TBSD 768552
12 February 2013
Initial
CE: RS QA: PJ
Coll: QC:

Journal of Biomolecular Structure and Dynamics, 2013
Vol. X, No. X, 0–17, http://dx.doi.org/10.1080/07391102.2013.768552

Taylor & Francis
Taylor & Francis Group

Molecular dynamics simulations show how the FMRP Ile304Asn mutation destabilizes the KH2 domain structure and affects its function

Daniele Di Marino[a,b,c], Tilmann Achsel[a,b], Caroline Lacoux[a,b], Mattia Falconi[d,e] and Claudia Bagni[a,b]*

[a]*VIB Center for the Biology of Disease, Catholic University of Leuven, Herestraat 49, 3000 Leuven, Belgium;* [b]*Università di Roma Tor Vergata, via della Ricerca Scientifica 1 & via Montpellier 1, 00100 Rome, Italy;* [c]*Department of Physics, University of Rome "La Sapienza", P.le Aldo Moro, 5, 00185 Rome, Italy;* [d]*Department of Biology, University of Rome "Tor Vergata" and CIBB, Center of Biostatistics and Bioinformatics, via della Ricerca Scientifica, 00133, Rome, Italy;* [e]*Interuniversity Consortium, National Institute Biostructure and Biosystem (INBB), Viale delle Medaglie d'Oro 305, 00136 Roma, Italy*

(*Received 31 August 2012; final version received 16 January 2013*)

Mutations or deletions of FMRP, involved in the regulation of mRNA metabolism in brain, lead to the Fragile X syndrome (FXS), the most frequent form of inherited intellectual disability. A severe manifestation of the disease has been associated with the Ile304Asn mutation, located on the KH2 domain of the protein. Several hypotheses have been proposed to explain the possible molecular mechanism responsible for the drastic effect of this mutation in humans. Here, we performed a molecular dynamics simulation and show that the Ile304Asn mutation destabilizes the hydrophobic core producing a partial unfolding of two α-helices and a displacement of a third one. The affected regions show increased residue flexibility and motion. Molecular docking analysis revealed strongly reduced binding to a model single-stranded nucleic acid in agreement with known data that the two partially unfolded helices form the RNA-binding surface. The third helix, which we show here to be also affected, is involved in the PAK1 protein interaction. These two functional binding sites on the KH2 domain do not overlap spatially, and therefore, they can simultaneously bind their targets. Since the Ile304Asn mutation affects both binding sites, this may justify the severe clinical manifestation observed in the patient in which both mRNA metabolism activity and cytoskeleton remodeling would be affected.

Keywords: FMRP; KH domain; molecular dynamics simulation; protein–nucleic acid docking

Introduction

In brain, a variety of proteins contribute to the regulation of gene expression at post-transcriptional level: among the best characterized is the Fragile X mental retardation protein (FMRP) (Bagni, Tassone, Neri, & Hagerman, 2012; De Rubeis, Fernandez, Buzzi, Di Marino, & Bagni, 2012; Wang, Bray, & Warren, 2012). FMRP is an RNA-binding protein that forms messenger ribonucleoparticle (mRNP) shuttling from the soma to the synapses, in order to regulate multiple steps of mRNA metabolism, including dendritic transport, stability, and local translation(De Rubeis et al., 2012; Wang et al., 2012). Lack or mutations in FMRP lead the Fragile X syndrome (FXS), the most frequent form of intellectual disability (Hagerman, 1996; Jacquemont, Hagerman, Hagerman, & Leehey, 2007).The majority of FXS patients have an expanded CGG triplet in the 5′-untranslated region (UTR) of the Fragile X mental retardation gene FMR1 that leads to transcriptional silencing and the absence of the FMRP (Oberle et al., 1991; Verkerk et al., 1991). However, few cases of individuals carrying either deletions or point mutations within the FMR1 gene have also been reported (De Boulle et al., 1993; Hammond, Macias, Tarleton, & Shashidhar Pai, 1997).

FMRP has four independent RNA-binding domains. In mammals, FMRP is able to recognize a large number of mRNAs (Brown et al., 2001; Darnell et al., 2011; Miyashiro et al., 2003) and noncoding RNAs, including the brain cytoplasmic RNA BC1/BC200 (Johnson et al., 2006; Lacoux et al., 2012; Napoli et al., 2008; Zalfa et al., 2003) and some microRNAs (Edbauer et al., 2010; Muddashetty et al., 2011).

FMRP homodimerizes and interacts with several cytoplasmic and nuclear proteins, including the two paralogs FXR1P and FXR2P (Sjekloća et al., 2009; Tamanini et al., 1999; Zhang et al., 1995). FMRP, FXR1P, and FXR2P share a common structure consisting of a N-terminal domain with two Tudor motifs (Ramos et al., 2006), a linker domain with a potential helix-loop-helix motif (HLH) containing a nuclear localization signal

*Corresponding author. Email addresses: claudia.bagni@uniroma2.it

(NLS), a central region with two KH domains (KH1 and KH2) and a nuclear export signal (NES), and a C-terminus with a RGG box (Bagni & Greenough, 2005). Each of the four domains is able to bind RNA molecules individually (De Rubeis et al., 2012). The entire N-terminal region forms a novel RNA-binding domain that was shown to interact with polyribonucleotides (Adinolfi et al., 1999; Siomi, Choi, Siomi, Nussbaum, & Dreyfuss, 1994; Siomi, Zhang, Siomi, & Dreyfuss, 1996) as well with neuronal RNAs (Lacoux et al., 2012; Zalfa et al., 2003).The KH2 domain, located in the central portion of the protein, is responsible for the binding to a series of *in vitro* selected short RNAs characterized by a particular structure defined kissing complex (Darnell et al., 2005). Finally, the C-terminal region of FMRP has an RGG box crucial for the interaction with some mRNAs containing a G-quartet structure (Darnell et al., 2001; Schaeffer et al., 2001; Ramos, Hollingworth, & Pastore, 2003a, 2003b), with G-rich regions (Zalfa et al., 2007), with microRNAs (Muddashetty et al., 2011).

A few cases with *FMR1* deletions or a mosaic of a deletion and a full mutation in the FMR1 gene have also been described and lead to the same Fragile X phenotype (Gedeon et al., 1992; Lugenbeel, Peier, Carson, Chudley, & Nelson, 1995; Mila et al., 1996; Petek, Kroisel, Schuster, Zierler, & Wagner, 1999; Tarleton et al., 1993). The most severe and best-characterized point mutation identified so far is the Ile304Asn substitution in the KH2 domain of FMRP (De Boulle et al., 1993; Valverde, Edwards, & Regan, 2008; Valverde, Pozdnyakova, Kajander, Venkatraman, & Regan, 2007). The patient with FXS and such a mutation has a severe form of intellectual disability, a pronounced macroorchidism and a severe social and behavioral impairment (De Boulle et al., 1993). Several studies have been carried out in order to clarify the effect that the Ile304Asn mutation has on the FMRP function. While FMRP carrying this mutation is still able to bind mRNAs-containing a G-quartet, its binding to the kissing complex structure is reduced (Darnell et al., 2005). Furthermore, studies performed in neurons did not show any difference in FMRP Ile304Asn granular labeling and transport to dendrites (Castrén, Haapasalo, Oostra, & Castrén, 2001) neither in the binding to FXR1P. Finally, the human Ile304Asn FMRP forms mRNPs altered in mass and density (Feng et al., 1997), retains *in vitro* RNA binding to poly(G) homopolymer but exhibits reduced binding to poly(U) homopolymer (Brown et al., 1998; Siomi et al., 1994).

One of the modes FMRP regulates mRNA metabolism is as repressor of translational initiation *in vitro* (Laggerbauer, Ostareck, Keidel, Ostareck-Lederer, & Fischer, 2001) as well as at neuronal synapses (Zalfa et al., 2003). Importantly, Laggerbauer and colleagues showed that FMRP Ile304Asn fails to suppress translational initiation (Laggerbauer et al., 2001). In addition to the effect on the mRNA targets, it has been recently shown that both FMRP and FXR1P KH2 domains are able to bind the Cdc42 effector PAK1 and that FXR1 (I304 N) fails to bind PAK1 (Say et al., 2010).

Circular dichroism (CD) spectra and melting curves of KH domains containing the Ile304Asn mutation showed a partial unfolding of the domain (Musco et al., 1997; Pozdnyakova & Regan 2005; Ramos et al., 2003a, 2003b; Valverde et al., 2007). However, the precise effect of the mutation on the structure is not known and can be only speculated if it primarily affects (a) the intra and/or intermolecular interactions of FMRP; or (b) it might impair FMRP's interactions with its RNA target(s).

Here, we clarified the structural rearrangements that the KH2 domain undergoes as a consequence of the Ile304Asn mutation using molecular dynamics (MD) and show that the mutation slightly opens the hydrophobic core and distorts the nucleic acid-binding site. Consequently, docking simulations show reduced affinity to nucleic acid.

Materials and methods

MD simulation

Forty nano second MD simulations of the FMRP KH2 domain and the Ile304Asn mutant have been carried out with the GROMACS MD package version 4.0.7 (Van Der Spoel et al., 2005). Initial coordinates of the sole KH2 domain were taken from the 2QND PDB file, which contains the structure of human FMRP KH1-KH2 (Valverde et al., 2007). Thus, the KH2 domain variable loop was not completely resolved due to its length and degree of flexibility; in this study, we have used the structure of the KH2 domain with a shorter variable loop, reconstructed by the crystallographers (Valverde et al., 2007). The whole system consisted of the FMRP KH2 domain molecule immersed in a box filled by 6057 SPC water molecules (Darden, York, & Pedersen, 1993). One solvent molecule was replaced by one Na^+ counterion to keep the system electrically neutral. Long-range electrostatic interactions were calculated using the Particle-Mesh Ewald summation method (Berendsen, Grigera, & Straatsma, 1987), while short-range interactions were taken into account by using 1.0 nm cutoff method. All bonds were constrained using the LINCS algorithm (Hess, Bekker, Berendsen, & Fraaije, 1997).

The overall thermalization procedure was as follows: the initial structure was subjected to a cycle of energy minimization of the solvent and protein using the steepest descent algorithm with 100 $kJ\,mol^{-1}\,nm^{-1}$ tolerance, using a step of 0.01 nm and position restraints on the protein. A 100 ps restrained MD at 300 K was then performed to equilibrate the water molecules around the protein, followed by a second cycle of steepest descent

energy minimization of 1000 steps on the whole system with no restraints. Temperature was raised up to the final 300 K value in a stepwise manner. A series of 50 ps MD runs at the increasing temperature of 50, 100, 200, and 250 K have been carried out. The system has been then simulated for 40 ns at a constant temperature of 300 K using the Berendsen's method (Berendsen, Postma, van Gunsteren, Di Nola, & Haak, 1984) and at the constant pressure of 1 bar kept constant using the Rahman-Parrinello barostat (1981) with a 2.0 fs time step. All coordinates were saved every 0.25 ps. In order to evaluate the structural perturbations induced by the Ile304Asn mutation on the native KH2 structure, the last structure of the wild-type protein that appeared with the MD simulation (i.e. the structure taken at 40 ns) has been used to start the simulation of the FMRP Ile304Asn mutant. The isoleucine 304 has been mutated into asparagine using the SwissPDB-Viewer program (Guex & Peitsch, 1997). After the residue substitution, another 100 ps restrained MD at 300 K was performed to equilibrate the water molecules around the KH2 mutant structure. The KH2 domain with the Ile304Asn mutation was simulated for 40 ns under the same conditions previously described for the simulation of the wild-type protein. The first 10 ns of both simulations were discarded to take into account the long-system equilibration. Root mean square deviations (RMSD) and per-residue root mean square fluctuations (RMSF) trajectory analyses were performed by using the available GROMACS analysis tools (Hess, Kutzner, van der Spoel, & Lindahl, 2008). Solvent-accessible surface (SAS) has been calculated with the program Naccess (Hess et al., 2008; Hubbard & Thornton, 1993), iteratively run using in house perl written code. CD spectrum for the last structure extracted from the simulations of the wild-type and mutant FMRP KH2 domain has been simulated using the DichroCalc server (http://comp.chem.nottingham.ac.uk/dichrocalc) (Bulheller & Hirst, 2009).

Principal component analysis

The Principal component analysis (PCA) (essential dynamics) analysis (García, 1992) has been performed as previously described (Di Marino, Oteri, Morozzo Della Rocca, Chillemi, & Falconi, 2010). Briefly, higher frequency fluctuations have been filtered out by diagonalization of atomic positional fluctuations covariance matrix calculated during the production run and the corresponding eigenvectors; eigenvalues have been used to describe large-amplitude motions (Garcia, 1992).

Cumulative correlation analysis

The dynamic cumulative correlation analysis of the systems were carried out with in-house written code, taking into account only the $C\alpha$ atoms coordinates that contain enough information to describe the largest system motions. The elements of the cumulative correlation analysis (C_{ij}) were computed as follows:

$$\frac{C_{ij} = \langle \Delta r_i \times \Delta r_j \rangle}{\left(\sqrt{\langle \Delta r_i^2 \rangle} \times \sqrt{\langle \Delta r_i^2 \rangle} \right)}$$

where Δr_i is the displacement from the mean position of the ith atom and the $\langle\rangle$ represent the time average over the whole trajectory.

Positive C_{ij} values represent a correlated motion between residues i and j (i.e. the residues move in the same direction). Negative values of C_{ij} represent an anti-correlated motion between residues i and j (i.e. they move in opposite directions). Cumulative positive and cumulative negative correlations were computed by adding separately the positive and negative terms. Graphs were obtained with Grace-5.1.10 (http://plasma-gate.weizmann.ac.il/Grace/) program and images with the MacPyMol (http://www.pymol.org) (DeLano, 2002).

Molecular docking

In order to assess the ability of the FMRP KH2 and FMRP KH2 Ile304Asn domains to bind ssDNA or RNA substrates, two different docking experiments have been performed. For the docking with ssDNA, we have chosen as referring structure for our modeling studies, the hnRNPK KH3 structure, since the structural alignment revealed an RMSD value between the hnRNPK KH3 and the FMRP KH2 structures of 1.8 Å. The DNA molecule for the docking simulations (sequence 5′-TCCCT-3′) has been extracted from the available 3-D structure of the hnRNP K KH3 domain (PDB code 1J5 K) (Braddock, Baber, Levens, & Clore, 2002; Braddock, Louis, Baber, Levens & Clore, 2002). A sequence alignment between FMRP KH2 and hnRNPK KH3 domains was performed with the program Needle (http://www.ebi.ac.uk/Tools/emboss/align/index.html), obtaining an identity and a similarity of 28 and 49%, respectively. Furthermore, the 3-D structures of these two domains have been aligned with the DaliLite web server v. 3 (Holm & Rosenstrom, 2010) in order to evaluate the structural similarity of the two domains.

For the docking with RNA, we have chosen as a reference structure the Nova-2 KH3 domain, cocrystallized with a 20 nucleotide RNA molecule(5′-GAGGACCUAGAUCACCCCUC-3′) (PDB code 1EC6) (Lewis et al., 2000). The sequence alignment between FMRP KH2 domain and Nova-2 shows an identity and similarity of 24 and 38%, respectively, and the structural alignment revealed an RMSD value between Nova-2 and the FMRP KH2 structure of 2.6 Å.

The wild-type and mutant KH2 structures used as docking partners have been extracted upon clustering of the two simulations. The clustering has been performed

with the GROMACS g cluster tool, using the GROMOS method with a cutoff of 1.8 Å. The clustering gave rise to 1 cluster for the wild type and to 12 clusters for the mutant. In the mutant, the centroid of cluster two has been selected for the docking, since the structures belonging to this cluster correspond to the time window comprised between 28 and 40 ns (Figure S1), after the unfolding.

The wild-type and mutant KH2 structures used as docking partners have been extracted at 40 ns, that is, the last frame of the trajectories. The docking simulations, of 50 runs each, have been performed using the HADDOCK program (Dominguez, Boelens, & Bonvin, 2003) particularly suitable for the nucleic acids docking. The structure with the smallest weighted sum has been ranked first. The results of the docking runs have been clustered based on the RMSD criterion, using a 4.5 Å cutoff. The effect of the mutations has been quantified considering the HADDOCK score, that is calculated according to the weighted sum of various energy terms: van der Waals, electrostatic, restraints, diffusion anisotropy, dihedral angle restraints, symmetry restraints, buried surface area, binding and desolvation energies (see the HADDOCK manual for further information (Dominguez et al., 2003). Docking simulations of the wild-type and the mutant Ile304Asn with ssDNA have generated ten and nine families, respectively, while docking with RNA have generated seven and five families for the wild type and mutant, respectively. The complex with the best HADDOCK score (Dominguez et al., 2003) has been selected from the most populated families for each docking simulation. The docking results obtained for the FMRP KH2 domain have been compared with the hnRNPK KH3-DNA NMR structure (Braddock, Baber et al., 2002; Braddock, Louis et al., 2002) and the Nova-2 KH3-RNA X-ray structure (Lewis et al., 2000).

Results

Structural and dynamical analysis

The KH2 domain of FMRP is located in the central portion of the protein (Figure 1(A)) and is formed by the alternation of three α-helices (α1-α2-α′) and three β-strands (β1-β2-β′) (Figure 1(B)). Ile304 is located at the level of α-helix 2 (Figure 1(B) and (C)) and when mutated in asparagine causes a severe manifestation of the FXS (De Boulle et al., 1993).

The Ile304 substitution was introduced in the resolved structure of the KH2 domain (Valverde et al., 2007), and MD simulation was performed over 40 ns. The RMSD, measure of the average distance between the *C*α atoms of the simulated structure and starting structure, was calculated for the trajectories of wild-type and mutant KH2 domains and reported in Figure 2(A). The wild-type protein reaches a plateau after 10 ns, with an average value of 0.3 nm (Figure 2(A), black line). On the contrary, the RMSD of the Ile304Asn mutant grows up to 0.5 nm (Figure 2(A), gray line) indicating a destabilization of the entire domain structure.

In a similar way, analysis of the SAS shows a clear difference between the two simulations (Figure 2(B)). The value of the SAS calculated for the wild-type domain (black line) is fairly constant along all the simulation time and its average value is 14.6 nm^2, while the Ile304Asn mutant (gray line) fluctuates around an average of 16.3 nm^2. This indicates that the structure of the mutant is more relaxed and loses its compactness. The time dependence of the number of residues belonging to secondary structure elements is shown in Figure 2(C). The analysis indicates that the secondary structure content remains fairly constant along the trajectory in the wild-type simulation (black line), fluctuating around 60 of the 79 residues composing the KH2 domain. On the contrary, in the mutant protein, a partial loss of secondary structure occurs along the time evolution of the system and, at 40 ns (gray line) only 45 structured residues are left. In particular, helix α2 in the wild type is composed of three turns, two of which are lost along the simulation of the mutant due to loss of up to eight intrahelical hydrogen bonds (see below). In order to further validate our findings, we have simulated the CD spectrum (Bulheller & Hirst, 2009) of the structure after 40 ns of MD simulation (Figure 2(D)). Of note, the outcome nicely reproduces the experimental result by Valverde et al. (2007), indicating that our MD simulations are correctly sampling the physical behavior of the KH2 domain. Taken together, these results suggest that the Ile304Asn mutation induces a partial unfolding of the native KH2 domain.

Tertiary structure and hydrophobic core analyses

In order to detect which secondary structure elements are mainly affected by the mutation, the *C*α atoms of 4 snapshots, extracted every 10 ns from both the wild-type and mutant domain simulations, have been superposed and reported in orange and blue color, respectively (Figure 3 (A)). In the wild-type simulation, the helices α1, α2, and α′ maintain their structure and position along the entire trajectory. In the mutant domain, it appears that helices α1 and α2 are partially unfolded so that helix α′ is displaced from its original position causing the relaxation of the hydrophobic core. On the other hand, for both the wild-type and mutant proteins, the β-sheet region does not undergo significant changes over the simulation time.

To elucidate the molecular mechanism that induces unfolding of the KH2 domain, we monitored the distances between the hydrophobic residues of the α-helices and those of the β-sheet. The following residues form the hydrophobic core cluster: Val293, Val296, Leu303,

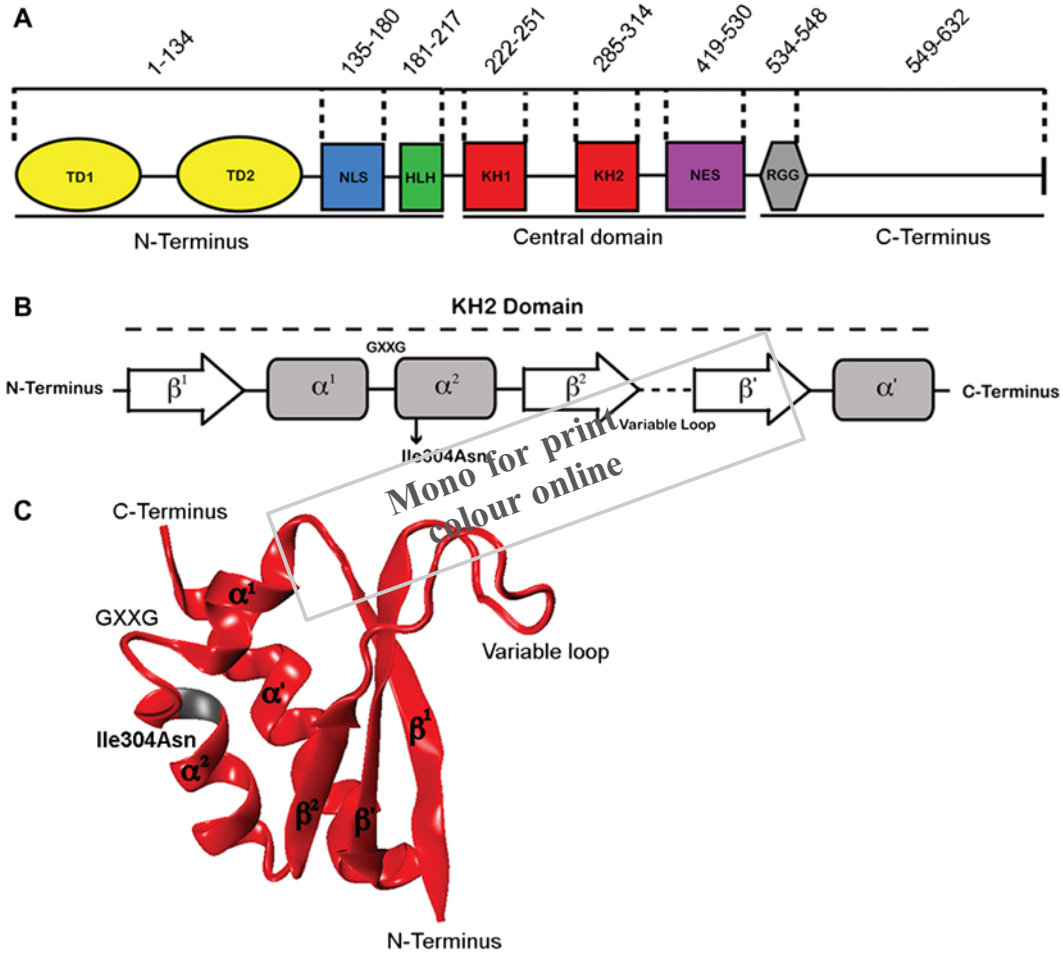

Figure 1. Protein topology and structure. (A) Schematic representation of the FMRP domains according to (Adinolfi et al., 1999), with the relative amino acid sequence number. The domains are reported with the following color code: Tudor domains 1 and 2 = yellow; NLS = blue; HLH motif = green; KH1 and KH2 = red; NES = violet; RGG box = gray. (B) Succession of the secondary structure elements composing the KH2 domain. (C) Three-dimensional structure from (Valverde et al., 2007) of the KH2 domain represented as a red ribbon. The secondary structure elements and the N-terminus and C-terminus are labeled. The position of the Ile304Asn mutation is reported in gray color on the red structure.

Ile304, Val308, and Leu358 for the α-helices and: Val316, Ile318, and Phe335 for the β-strands (Figure 3 (B)). The centers of mass of the amino acids on the α-helices and on the β-strands were calculated separately. Their distance defines the compactness of the hydrophobic core. Figure 3(C) shows that this distance is constant along the wild-type trajectory, while it notably increases for the mutant (Figure 3(C), black vs. gray line). The first interactions lost, along the simulation of the mutant, are those ofAsn304 (on the a2 helix) that looses the contact with Ile318 at around 6 ns and subsequently with Val316 and Phe380 (both on the β strands) at around 12 ns. Furthermore, Leu303 (located on α^2 helix) looses the interaction with Leu358 (on β′ strand) at around 22 ns (Figure S2).This pattern indicates how these residues play a crucial role in the maintenance of the hydrophobic core.

Per residue fluctuation analysis

Analysis of the average RMSF for each residue in both simulations is reported in Figure 4 and shows how the presence of the mutation (black dot) on helix 2 influences the mobility of the entire domain. The amino acid fluctuation for the wild-type trajectory is low for the residues that constitute the secondary structure elements, while it reaches higher values for the loops regions (Figure 4, black line). On the contrary, the fluctuation profile of the mutant shows a general increase for all the residues, indicating that a single mutation on helix 2 is able to significantly change the flexibility of the whole KH2 domain structure (Figure 4, gray line) and consequently decreases the domain stability. Large fluctuations occur just upstream and downstream of the Ile304Asn mutation (boxed with a dashed line), as well as in the α′ region (see discussion; see also Supplementary movies 1 and 2).

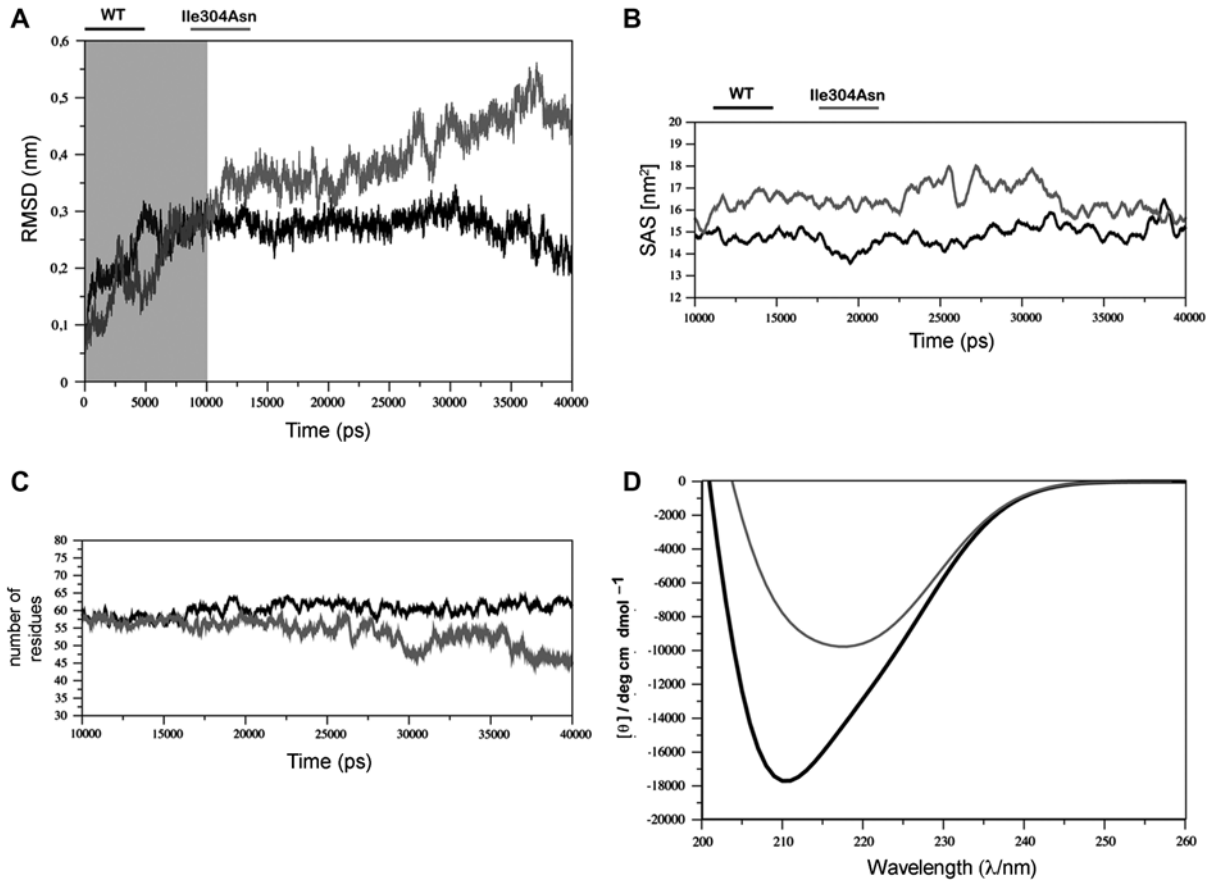

Figure 2. Analyses of domain structure stability. (A) RMSD calculated on the *C*α atoms along the 40 ns simulations. The gray box represents the equilibration time, which has not been considered for further analyses. (B) SAS. (C) Number of amino acids in secondary structure. (D) CD spectrum calculated on the 40 ns simulation structures. In all the graphs, the wild-type (WT) and mutant (Ile304Asn) values are reported in black and gray lines, respectively.

Principal component and correlated/anticorrelated motion analysis

The main dynamical features of the wild-type and the mutant domains have been investigated through the principal components analysis (PCA) on the atomic positional fluctuations covariance matrix of the *C*α atoms (Garcia, 1992). The analysis extracts from the complex fluctuations some simple underlying movements that are mathematically described by the so-called eigenvectors. Here, the first 10 eigenvectors describe, respectively, for the wild-type and the mutant simulations, about 75% and 85% of the total motion (Figure 5 (A)). In detail, the weight of the first eigenvector represents about 18 and 48% of the global fluctuations in the wild type and mutant, respectively (Figure 5(A)). The most significant eigenvector in the wild-type simulation mainly describes the motions of the loop (Figure 5 (B), amplitude of motion from blue to red), while there is little motion in the secondary structure elements (thin ribbons). On the contrary, in the mutant simulation, the first eigenvector indicates that also the motions of helices α2 and α′ significantly increase (Figure 5(C)), explaining a higher percentage, as compared to the wild type, of total motion description in the essential space (Figure 5(A)). The sum of correlated and anticorrelated motions that a specific residue establishes with all the other residues of the domain has been calculated and the result is shown in Figure 5(D). Specifically, the single mutation Ile304Asn causes a change in the profile of the cumulative correlation motions localized along the entire KH2 domain. In particular, the residues located on helix α2 that in the mutant protein harbors the mutation, increase the cumulative positive correlation profile compared with wild-type simulation. This result indicates a partial unfolding of this protein region, which is primarily involved in the interaction with nucleic acids. The loss of secondary structure allows this region to be more flexible and mobile compared with the wild-type domain.

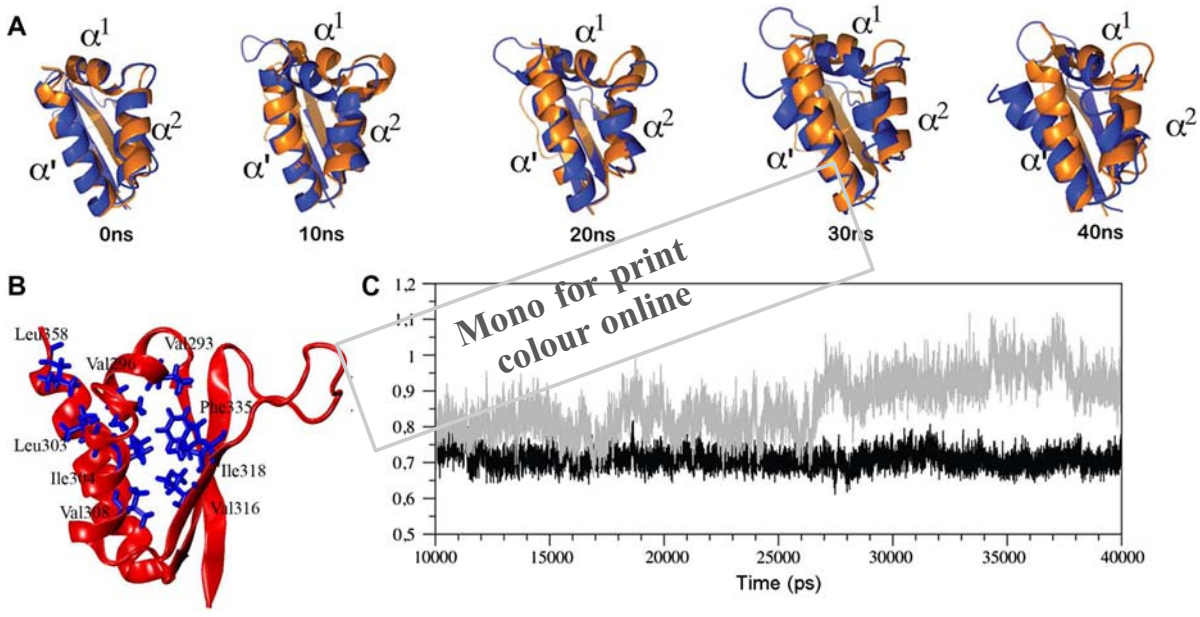

Figure 3. Hydrophobic core stability. (A) Structural superposition of the wild-type (orange) and mutant (blue) domains extracted from the trajectories every 10 ns. The helices are labeled. (B) Representative 3-D structure of the wild-type KH2 domain is reported as a red ribbon. The side chains of residues forming the hydrophobic core are reported in blue licorice, while the mutated residue, Ile304Asn, is reported in gray (C) Time evolution of the distance between the hydrophobic residues outlined in (B), in the wild type (black line) and in the mutant (gray line) simulations.

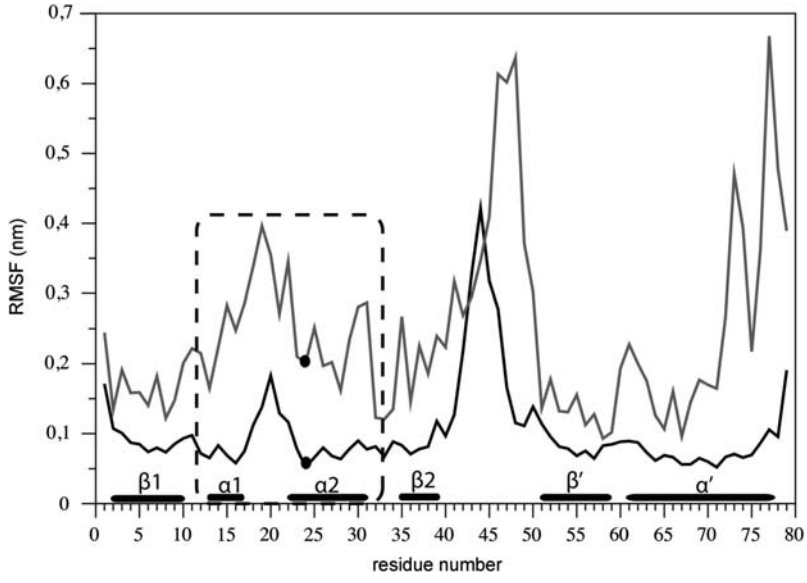

Figure 4. Residue flexibility. Average RMSF calculation for the wild-type (black line) and mutant domain (gray line) are reported for every residue. The black dot indicates the position of the mutated residue. The dashed line outlines the regions around the mutation. The secondary structures of the domain are reported at the bottom of the graph.

Docking simulations of FMRP-KH2 to nucleic acid

The interaction determinants of the eukaryotic KH domains with nucleic acids has been extensively studied and are found to be conserved (Adinolfi et al., 1999; Valverde et al., 2008).Sequence alignment between the FMRP KH2 and the hnRNPK KH3 domains revealed an identity of about 30% (Figure 6(A)). Moreover, the structural alignment between the two structures carried out using the DaliLite web server v.3 (Holm & Rosenstrom, 2010)gives an RMSD value of 1.8 Å (data not shown) and indicates that the residues directly involved in the RNA/DNA recognition (Figure 6(A), boxed in

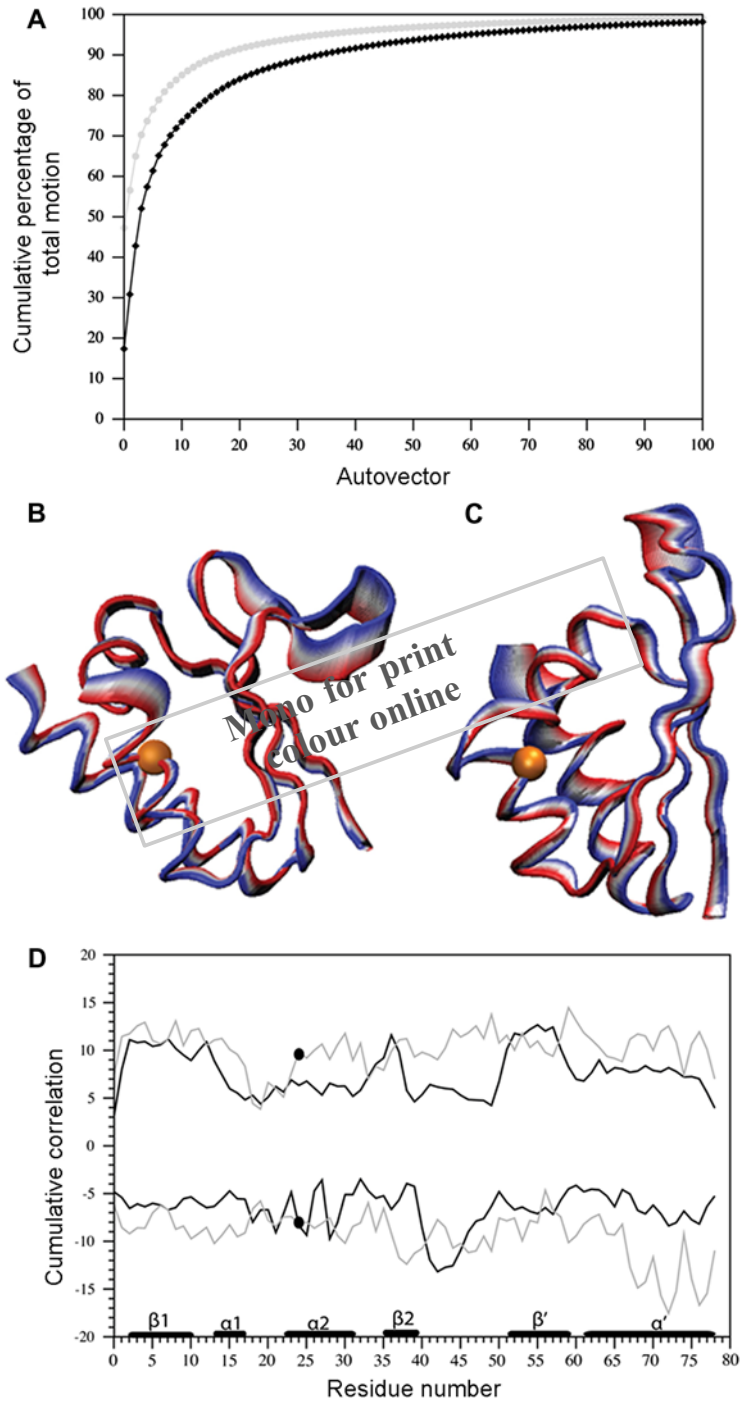

Figure 5. Domain concerted motion and PCA analysis. (A) Cumulative percentage of eigenvector weights in the wild-type (black) and mutant (gray) total motions. Projection of the motion along the first eigenvector for the wild type (B) and the mutant (C). The amplitude of the motion is reported with a color scale ranging from red to blue, while the residue of the mutation is indicated by an orange sphere. (D) Cumulative percentage of the positive and negative correlations of the motion between each residue and the rest of the domain. The black and gray lines represent the wild type and mutant, positive and negative, values of correlation for each residue, respectively. The black circle underlines residue 304, the secondary structures of the domain are also reported at the bottom of the graph.

gray) are conserved in both sequence and three-dimensional arrangement (Chothia & Lesk, 1986). The hnRNPK KH3 domain (Braddock, Baber et al., 2002; Braddock, Louis et al., 2002) has been selected as a structural template to study the nucleic acid binding properties of the FMRP KH2 domain because in this

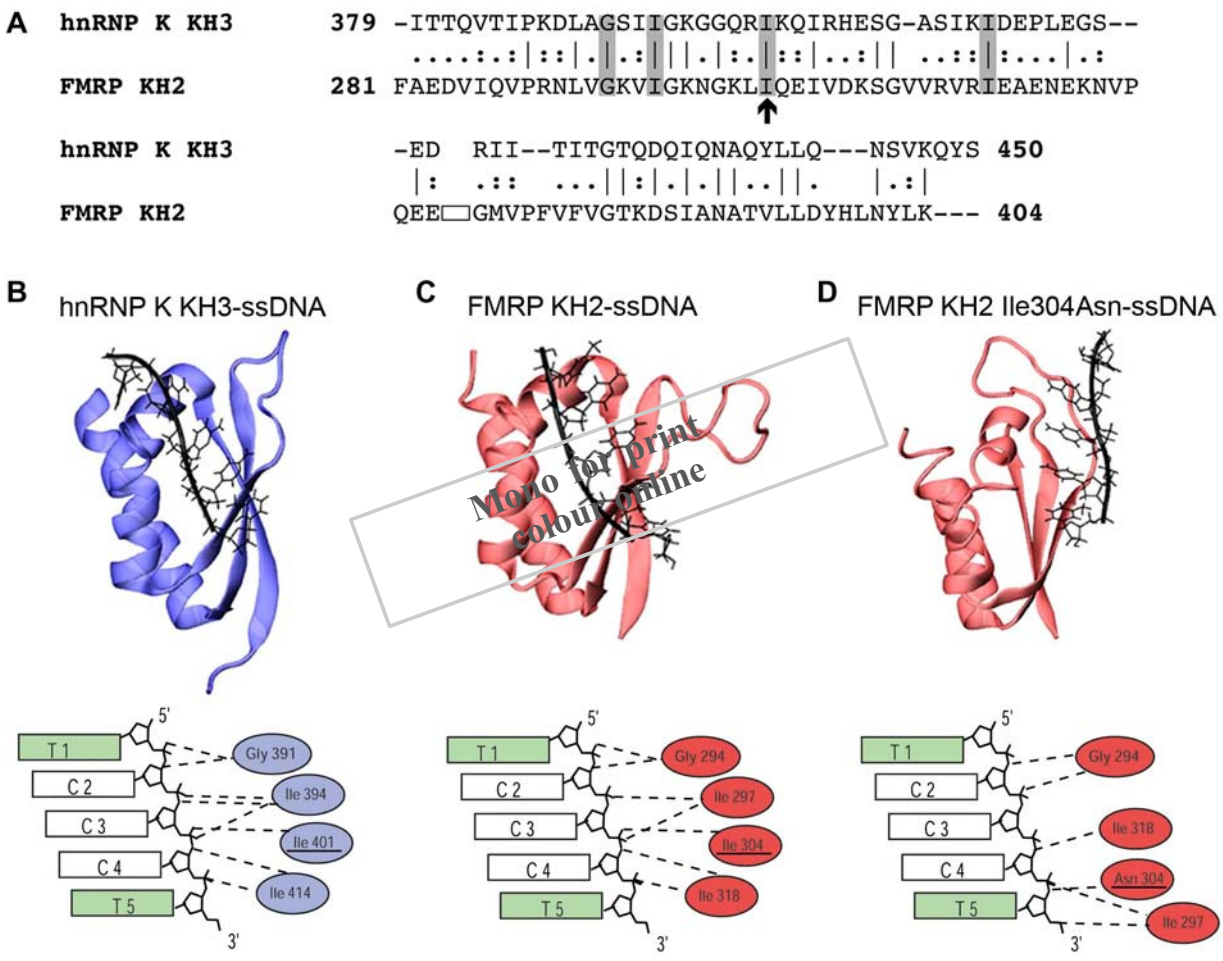

Figure 6. Docking experiments with ssDNA. (A) Sequence alignment between the hnRNP K KH3 and FMRP KH2 domains. The line, the double points and the point represent: identity, conservation and partial conservation of residues between the two sequences, respectively. The arrow indicates Ile304. The gray boxes underline the residues involved in the nucleic acid binding in the hnRNP K KH3 domain, also conserved in the FMRP KH2 domain. A white box indicates the variable loop position. (B) Upper panel: NMR structure of the hnRNP K KH3-ssDNA binary complex (Braddock et al., 2002). The protein domain is reported as a hazy blue ribbon, with the residues forming the nucleic acid (ssDNA) binding site shown as a black segment. (C) Upper panel: Wild type and (D) Upper panel: mutant KH2-ssDNA binary complex, obtained through molecular docking of the same ssDNA and the last structure extracted from the two simulations. In this context, the FMRP KH2 domain is in red. (B-C) Lower panels: Network of interaction between the ssDNA and the hnRNP K KH3, FMRP KH2, and FMRP KH2 Ile304Asn residues.

case a solution structure with a small ssDNA has been solved (Braddock, Baber et al., 2002; Braddock, Louis et al., 2002). Importantly, the same geometry of binding has also been found in other KH domains (Braddock, Baber, et al., 2002; Braddock, Louis, et al., 2002); FMRP binds to single-stranded DNA in addition to RNA (Ashley, Wilkinson, Reines, & Warren, 1993), similar to other RNP family proteins (Matunis, Michael, & Dreyfuss, 1992). In the case of hnRNPK, the conformation of RNA and ssDNA binding to the KH domain appears to be similar (Braddock, Baber et al., 2002; Braddock, Louis et al., 2002).

Based on these informations, we performed molecular docking simulations in order to verify if the FMRP KH2 wild-type and mutant structures maintain the interaction pattern observed in the hnRNPK KH3-ssDNA complex. The NMR structure of the hnRNP K KH3-nucleic acid complex is reported in Figure 6(B), while Figure 6(C) and (D) show the best FMRP KH2-nucleic acid complex obtained by docking simulations carried out on the most representative structure extracted from clustering the wild-type and the mutant trajectories, respectively (Figure S1). Main interactions stabilizing the hnRNPK KH3-ssDNA complex are represented by close contacts that occur between α-helix 1, in particular involving the Gly391 carbon atom belonging to the carbonyl group, and the T5 and C6 bases (Figure 6(B), DNA shown in black). Three isoleucines, 394, 401 and 414, are involved in the binding with bases C6, C7, and C8 forming a hydrogen bonds network. The analysis of

the FMRP KH2 wild-type domain-ssDNA complex shows that these interactions are also conserved between hnRNPK and FMRP domain (Figure 6(B) and (C)). This is due to the structural maintenance of all the residues that establish the hydrogen bonds network (Figure 6(B) and (C)). In detail, T5 and C6 are in close contact with Gly294 and C6, C7, and C8 are bound through a hydrogen bond network by Ile297, Ile304, and Ile318. Further, the distances between the atoms involved in the interactions between the residues and the nucleic acid are all lower than 4.5 Å, as those observed in the NMR reference structure (Braddock, Baber et al., 2002; Braddock, Louis et al., 2002).

On the contrary, the complex obtained using the mutant domain (Figure 6(D)) shows substantial differences when compared with the wild-type KH2 and with the hnRNPK KH3-ssDNA complexes. Indeed, the partial destabilization of the α-helices causes a different positioning of the ssDNA on the domain. In the mutant complex, the ssDNA structure appears shifted toward the top of the domain and less tightly bound by the protein, causing the loss of the interactions that are observed in the hnRNP K KH3-ssDNA NMR structure and are conserved in the wild-type FMRP KH2-ssDNA docked complex. Many of the interactions established in the wild type are lost in the mutant complex (Figure 6(C) and (D), lower panels) and in particular, Ile304Asn causes a deep change in the interaction profile. Moreover, the comparison of the HADDOCK (Dominguez et al., 2003) score is in line with the hypothesis that the mutant is less suitable for the interaction with the RNA/DNA. Actually, the best FMRP Ile304Asn mutant domain – ssDNA docking complex shows a HADDOCK score of −27.00, while the best FMRP WT domain – ssDNA complex has a value of −37.00. The higher HADDOCK value observed for the complex with the mutant domain is mainly due to the unfolding of the structure that, abolishing the shape complementarity, increases the binding energy.

The Nova-2 KH3 domain binds with high affinity and *in vitro* selected sequence, the structure that was determined by a cocrystal (Lewis et al., 2000). We next performed a docking experiment using a 20 nucleotide long RNA bearing that sequence (see Methods). FMRP-KH2 and Nova-2 KH3 share 24% of sequence identity (Figure 7(A)) and the structural alignment gives rise to an RMSD value of 2.6 Å. Among the 20 nucleotides (nt) of this RNA, the sequence AUCAC (nt 11–15) is crucial for the binding with Nova-2 KH3 (Lewis et al., 2000). Interestingly, the binding of Nova-2 involves residue Leu28 that corresponds to FMRP KH2 Ile304. As shown in Figure 7, our RNA-KH2 complexes (WT and Ile304Asn) have been compared with the Nova-2 KH3-RNA complex resolved by a crystal structure (Lewis et al., 2000). Figure 7(B) shows the crystal structure of the Nova-2 KH3-RNA, while Figure 7(C) and (D) show the complexes obtained for the wild-type and mutant KH2 (right panel) with the docking having HADDOCK scores of −104 and −87, respectively. While the binding mode between Nova-2 KH3/RNA and FMRP KH2/RNA is conserved (compare Figure 7(B) and (C)), the binding of FMRP KH2 I304 N/DNA or RNA is completely changed (Figures 6D and 7(D)). In the case of the WT KH2, most of the interactions occur at the level of nt 11–15, while for the Ile304Asn KH3, the majority of the interactions are found at the level of nt 1–5 and only few interactions involve nt 11–15 (Figures 6(C) and (D) and 7(C) and (D)).

Discussion

The Ile304Asn mutation, located on α-helix 2 of the KH2 domain of FMRP, gives rise to a severe manifestation of the FXS (De Boulle et al., 1993). The cause of the FMRP dysfunction due to such a mutation is still not clear; it could be impaired nucleic acidic recognition (Darnell et al., 2005; Feng et al., 1997; Musco et al., 1997; Ramos et al., 2003a, 2003b; Siomi et al., 1994; Valverde et al., 2007) or a defect in protein binding (Say et al., 2010). Preliminary biophysical experiments showed that the mutation somehow destabilizes the KH2 domain.

MD and docking studies are valid tools to identify the structural/functional consequences of a mutation (Cambria, Di Marino, Falconi, Garavaglia, & Cambria, 2010; Chillemi et al., 2008; Di Marino et al., 2010). Here, we use these simulations todissect, at atomic level, the structural/dynamic consequences induced by the Ile304Asn mutation on the KH2 domain and its effects on nucleic acid binding. The 40 ns MD simulation of the wild-type KH2 domain shows that the compactness of the hydrophobic core is maintained for the entire trajectory, while the mutation of Ile304Asn destabilizes the hydrophobic core producing a partial unfolding of the domain (Figures 2 and 5 and Figure S2). Specifically, the RMSD analysis shows that the structure of the Ile304Asn mutant domain is unable to reach the equilibrium, also after 40 ns of simulation, while the wild-type domain reaches the stability after 10 ns (Figure 2(A)). At the same time the SAS of the domain is higher indicating an opening of the structure (Figure 2(B)). The reduced compactness of the hydrophobic core leads to augmented fluctuation (Figure 4), increased internal motion (Figure 5(B)–(C) and Supplementary movies S1 and S2), and impaired correlation of internal motion in the most affected regions (Figure 5 (D)). With our approach we are therefore able to see, in atomic detail, where the unfolding occurs and which part of the KH2 domain shows increased movement/dynamics.

A KH domain is a conserved compact structure of three α-helices and three β-strands (Adinolfi et al., 1999;

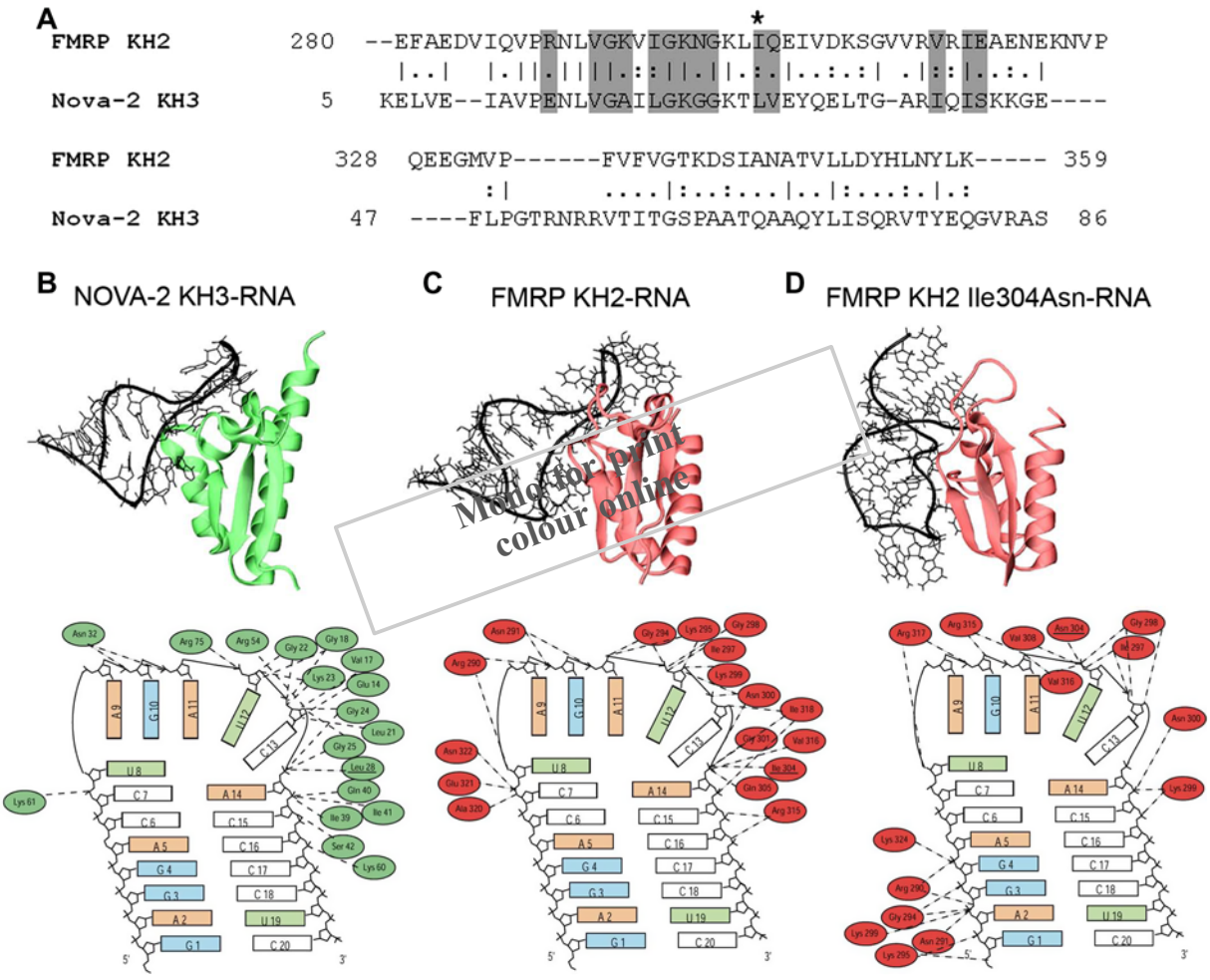

Figure 7. Docking experiments with RNA. (A) Sequence alignment between the Nova-2 KH3 and FMRP KH2. The line, the double points and the point represent: identity, conservation and partial conservation of residues between the two sequences, respectively. The arrow indicates Ile304. The gray boxes underline the residues involved in the nucleic acid binding in the hnRNP K KH3 domain, also conserved in the FMRP KH2 domain. (B) Upper panel: crystal structure of the Nova-2 KH3 (green ribbon) -RNA (black segment) (Lewis et al., 2000) (C) Upper panel: FMRP KH2 (red ribbon) and (D) FMRP KH2 I304 N-RNA binary complex, obtained through molecular docking of the same RNA and the last structure extracted from the two simulations are reported in red. Lower panels: Network of interaction between the RNA and the Nova-2 KH3, FMRP KH2, and FMRP KH2 Ile304Asn residues.

Valverde et al., 2008). Importantly, we highlight here that the unfolding process does not involve the entire domain. The sequence of events (Figure 3(A)) shows a primary unfolding of the α1 and α2 helices followed by a deviation of the α′ helix from its original structural position. The β-strands instead remain relatively stable. This process is caused by the substitution of the hydrophobic isoleucine with the polar asparagine, which impairs the network of hydrophobic interactions in the domain core (Figure 3(B)). Loss of two interactions of residue 304 with Leu318 and Val316 is the initial event of the unfolding (Figure S2). The primary effect of the Ile304Asn mutation is therefore a relaxation of the KH2 fold and the biological effects such as impaired nucleic acid or protein binding would be a consequence of the relaxation. Our structural model is validated by CD spectra experimentally observed for the mutant proteins (Musco et al., 1997; Ramos et al., 2003a, 2003b; Valverde et al., 2007) that suggest apartial loss of helicity.

To analyze the contribution of the mutated KH2 domain, we performed docking simulations between our structural model and a short ssDNA or RNA, using the NMR structure of KH3 domain of hnRNP K with the same ssDNA as a paradigm in one case (Backe, Messias, Ravelli, Sattler, & Cusack, 2005; Braddock et al., 2002) and the crystal structure of the KH3 domain of Nova-2 with a short RNA in the other (Lewis et al., 2000). The docking simulation (Figure 6) predicts that the FMRP KH2 domain can likewise stably associate to the model ssDNA or RNA, which is achieved mainly through complementarity to the surface of the α1 and α2 helices and the adjacent β strand for the binding with the DNA and

through the GXXG and variable loop structures for the binding with RNA. In the case of the DNA binding, the proper shape of the binding surface is ensured by a group of hydrophobic interactions and Ile304, although forming only a single hydrogen bond with the ssDNA (Figure 6) is strictly required to maintain the correct folding of the binding site. Consequently, docking simulation of the ssDNA to the mutated KH2 structure predicts a strong reduction in binding (Figure 6(D)). In the same way, the binding mode of the KH2 domain with the RNA is comparable with the one observed for Nova-2. In this case, the correct interaction is altered by the introduction of the asparagine in position 304 (Figure 7 (D)). Interestingly, Lewis and colleague had hypothesized that the Ile304Asn mutation could affect the binding of the FMRP-KH2 domain to the RNA (Lewis et al., 2000), and indeed, our analyses confirms this hypothesis.

From this analysis, we suggest that the mutated KH2 domain has a drastically decreased DNA-/RNA-binding capacity as a consequence of the partial unfolding of the α1/α2 helices; FMRP is a multidomain protein, including four RNA-binding domains (De Rubeis et al., 2012) and therefore a platform for multiple RNA and protein interactions (Wang et al., 2012). It is tempting to hypothesize that the types of RNA that still bind to mutant FMRP, such as poly(rG) (Brown et al., 1998; Siomi et al., 1994), bind to one of the other RNA-binding domains present in the full-length protein.

Interestingly, very recently, it has been observed that the KH2 domain of FXR1 and FMRP can also bind the PAK1 (p21 protein -Cdc42/Rac – activated kinase 1) protein (Say et al., 2010). The interaction occurs mainly with the α′ helix (Say et al., 2010) which, in our simulation, loses its spatial anchor due to the loosening of the hydrophobic core. In agreement with our analysis, the Ile to Asn mutation abolishes PAK1 binding (Say et al., 2010).

The partial unfolding of the mutated KH2 domain is mainly due to the destabilization of the hydrophobic cluster between helices α1, α2, and β2, β′ which is crucial for the correct arrangement of the nucleic acids binding sites. It is tempting to speculate that mimicking the presence of the isoleucine in position 304 in the mutant protein could protect the domain from unfolding. Future investigations might identify compounds able to restore the hydrophobic cluster altered by the mutation. This compound, interacting with the asparagine, should stabilize the pocket, and hence, the entire KH2 domain, in a conformation, that is similar to the wild type, restoring its ability to bind nucleic acids.

The docking analysis allows to hypothesize a mechanism of selection for the interaction of the FMRP-KH2 domain with DNA or RNA molecules. The interaction between KH2 and the ssDNA involves 4 bases and 4 amino acids with 3 hydrophobic residues and a glycine establishing hydrogen bonds with the bases (Figure 6). The docking performed on the basis of the Nova-2 KH3-RNA cocrystal (Lewis et al., 2000), suggest that this scheme is still present (Figure 7), but is greatly improved due to the high structural complexity of the RNA (Braddock et al., 2002). Since other domains of FMRP are able to interact with nucleic acids (Bagni et al., 2012; Lacoux et al., 2012), the ability of the protein to discern between different sequences could be an effect of the cooperation of KH2 with other FMRP domains.

In conclusion, this study suggests that the opened hydrophobic core, consequence of the asparagine insertion, affects the shape of two distinct interaction surfaces of the KH2 domain: the one binding to nucleic acids and the other binding to PAK1 protein. The two activities of the KH2 domain are not mutually exclusive and their convergence may justify the severe clinical manifestation observed in the patient (De Boulle et al., 1993) in which both mRNA metabolism activity and cytoskeleton remodeling would be affected.

Acknowledgments

We would like to thank Christian Seeger, Matthis Geitmann and HelenaDanielson from BEACTICA for sharing some preliminary data. This study was supported by Telethon (GGP10150), FWO (G066709N), VIB, HEALTH-2009-2.1.2-1 EU-FP7 ‘SynSys’ and Queen Elisabeth Foundation (FMRE, Belgium) to (CB).

Supplementary material

The supplementary material for this paper is available online at http://dx.doi.org/10.1080/07391102.2013.768552.

References

Adinolfi, S., Bagni, C., Castiglione Morelli, M. A., Fraternali, F., Musco, G., & Pastore, A. (1999). Novel RNA-binding motif: the KH module. *Biopolymers, 51*, 153–164.

Adinolfi, S., Bagni, C., Musco, G., Gibson, T., Mazzarella, L., & Pastore, A. (1999). Dissecting FMR1, the protein responsible for Fragile X syndrome, in its structural and functional domains. *RNA, 5*, 1248–1258.

Ashley, C. T.Jr., Wilkinson, K. D., Reines, D., & Warren, S. T. (1993). FMR1 protein: Conserved RNP family domains and selective RNA binding. *Science, 262*, 563–566.

Backe, P. H., Messias, A. C., Ravelli, R. B., Sattler, M., & Cusack, S. (2005). X-ray crystallographic and NMR studies of the third KH domain of hnRNP K in complex with single-stranded nucleic acids. *Structure, 13*, 1055–1067.

Bagni, C., & Greenough, W. T. (2005). From mRNP trafficking to spine dysmorphogenesis: the roots of fragile X syndrome. *Nature Reviews Neuroscience, 6*, 376–387.

Bagni, C., Tassone, F., Neri, G., & Hagerman, R. (2012). Fragile X syndrome: Causes, diagnosis, mechanisms, and therapeutics. *Journal of Clinical Investigation, 122*, 4314–4322.

Berendsen, H. J. C., Grigera, J. R., & Straatsma, T. P. (1987). The missing term in effective pair potentials. *Journal of Physical Chemistry, 91*, 3.

AQ2 Berendsen, H. J. C., Postma, J. P. M., van Gunsteren, W. F., Di Nola, A., & Haak, J. R. (1984). Molecular dynamics with coupling to an external bath. *Journal of Chemical Physics, 81*, 7.

Braddock, D. T., Baber, J. L., Levens, D., & Clore, G. M. (2002a). Molecular basis of sequence-specific single-stranded DNA recognition by KH domains: Solution structure of a complex between hnRNP K KH3 and single-stranded DNA. *EMBO, J21*, 3476–3485.

Braddock, D. T., Louis, J. M., Baber, J. L., Levens, D., & Clore, G. M. (2002). Structure and dynamics of KH domains from FBP bound to single-stranded DNA. *Nature, 415*, 1051–1056.

Brown, V., Jin, P., Ceman, S., Darnell, J. C., O'Donnell, W. T., Tenenbaum, S. A., … Warren, S.T. (2001). Microarray identification of FMRP-associated brain mRNAs and altered mRNA translational profiles in fragile X syndrome. *Cell, 107*, 477–487.

Brown, V., Small, K., Lakkis, L., Feng, Y., Gunter, C., Wilkinson, K. D., & Warren, S. T. (1998). Purified recombinant Fmrp exhibits selective RNA binding as an intrinsic property of the fragile X mental retardation protein. *Journal of Biological Chemistry, 273*, 15521–15527.

Bulheller, B. M., & Hirst, J. D. (2009). DichroCalc-circular and linear dichroism online. *Bioinformatics, 25*, 539–540.

Cambria, M. T., Di Marino, D., Falconi, M., Garavaglia, S., & Cambria, A. (2010). Docking simulation and competitive experiments validate the interaction between the 2,5-xylidine inhibitor and Rigidoporus lignosus laccase. *Journal of Biomolecular Structure and Dynamics, 27*, 501–509.

Castrén, M., Haapasalo, A., Oostra, B. A., & Castrén, E. (2001). Subcellular localization of fragile X mental retardation protein with the I304N mutation in the RNA-binding domain in cultured hippocampal neurons. *Cellular and Molecular Neurobiology, 21*, 29–38.

Chillemi, G., D'Annessa, I., Fiorani, P., Losasso, C., Benedetti, P., & Desideri, A. (2008). Thr729 in human topoisomerase I modulates anti-cancer drug resistance by altering protein domain communications as suggested by molecular dynamics simulations. *Nucleic Acids Research, 36*, 5645–5651.

AQ3 Chothia, C., & Lesk, A. M. (1986). The relation between the divergence of sequence and structure in proteins. *EMBO Journal, 5*, 4.

Darden, T., York, D., & Pedersen, L. (1993). Particle mesh Ewald: An N-log(N) method for Ewald sums in large systems. *Journal of Chemical Physics, 98*, 4.

AQ4 Darnell, J. C., Fraser, C. E., Mostovetsky, O., Stefani, G., Jones, T. A., Eddy, S. R., & Darnell, R. B. (2005). Kissing complex RNAs mediate interaction between the Fragile-X mental retardation protein KH2 domain and brain polyribosomes. *Genes & Development–*.

Darnell, J. C., Jensen, K. B., Jin, P., Brown, V., Warren, S. T., & Darnell, R. B. (2001). Fragile X mental retardation protein targets G quartet mRNAs important for neuronal function. *Cell, 107*, 489–499.

Darnell, J. C., Van Driesche, S. J., Zhang, C., Hung, K. Y., Mele, A., Fraser, C. E., … Darnell, R. B. (2011). FMRP stalls ribosomal translocation on mRNAs linked to synaptic function and autism. *Cell, 146*, 247–261.

De Boulle, K., Verkerk, A. J., Reyniers, E., Vits, L., Hendrickx, J., Van Roy, B., … Willems, P.J. (1993). A point mutation in the FMR-1 gene associated with fragile X mental retardation. *Nature Genetics, 3*, 31–35.

De Rubeis, S., Fernandez, E., Buzzi, A., Di Marino, D., & Bagni, C. (2012). Molecular and cellular aspects of mental retardation in the Fragile X syndrome: From gene mutation/s to spine dysmorphogenesis. *Advances in Experimental Medicine and Biology, 970*, 517–551.

DeLano, W. L. (2002). *The PyMOL molecular graphics system*. San Carlos, CA: DeLano Scientific.

Di Marino, D., Oteri, F., Morozzo Della Rocca, B., Chillemi, G., & Falconi, M. (2010). ADP/ATP mitochondrial carrier MD simulations to shed light on the structural-dynamical events that, after an additional mutation, restore the function in a pathological single mutant. *Journal of Structural Biology, 172*, 225–232.

Dominguez, C., Boelens, R., & Bonvin, A. M. (2003). HADDOCK: A protein−protein docking approach based on biochemical or biophysical information. *Journal of the American Chemical Society, 125*, 1731–1737.

Edbauer, D., Neilson, J. R., Foster, K. A., Wang, C. F., Seeburg, D. P., Batterton, M. N., … Sheng, M. (2010). Regulation of synaptic structure and function by FMRP-associated microRNAs miR-125b and miR-132. *Neuron, 65*, 373–384.

Feng, Y., Absher, D., Eberhart, D. E., Brown, V., Malter, H. E., & Warren, S. T. (1997). FMRP associates with polyribosomes as an mRNP, and the I304N mutation of severe fragile X syndrome abolishes this association. *Molecular Cell, 1*, 109–118.

García, E. (1992). Large-amplitude nonlinear motions in proteins. *Physical Review Letters, 68*, 2696–2699.

Gedeon, A. K., Baker, E., Robinson, H., Partington, M. W., Gross, B., Manca, A., … Sutherland, G. R. (1992). Fragile X syndrome without CCG amplification has an FMR1 deletion. *Nature Genetics, 1*, 341–344.

Guex, N., & Peitsch, M. C. (1997). SWISS-MODEL and the Swiss-Pdb viewer: An environment for comparative protein modeling. *Electrophoresis, 18*, 2714–2723.

Hagerman, R. J. (1996). Fragile X syndrome. *Mental Retardation, 5*, 895–910.

Hammond, L. S., Macias, M. M., Tarleton, J. C., & Shashidhar Pai, G. (1997). Fragile X syndrome and deletions in FMR1: New case and review of the literature. *American Journal of Medical Genetics, 72*, 430–434.

Hess, B., Bekker, H., Berendsen, H. J. C., & Fraaije, J. (1997). LINCS: A linear constraint solver for molecular simulations. *Journal of Computational Chemistry, 18*, 10.

Hess, B., Kutzner, C., van der Spoel, D., & Lindahl, E. (2008). GROMACS 4: Algorithms for highly efficient, load-balanced, and scalable molecular simulation. *Journal of Chemical Theory and Computation, 4*, 13.

Holm, L., & Rosenstrom, P. (2010). Dali server: Conservation mapping in 3D. *Nucleic Acids Research, 38*, W545–W549.

Hubbard, S. J., & Thornton, J. M. (1993). *NACCESS' computer program, department of biochemistry and molecular biology*University College London. AQ5

Jacquemont, S., Hagerman, R. J., Hagerman, P. J., & Leehey, M. A. (2007). Fragile-X syndrome and fragile X-associated tremor/ataxia syndrome: Two faces of FMR1. *The Lancet Neurology, 6*, 45–55.

Johnson, E. M., Kinoshita, Y., Weinreb, D. B., Wortman, M. J., Simon, R., Khalili, K., … Gordon, J. (2006). Role of Purα in targeting mRNA to sites of translation in hippocampal neuronal dendrites. *Journal of Neuroscience Research, 83*, 929–943.

AQ6

Lacoux, C., Di Marino, D., Pilo Boyl, P., Zalfa, F., Yan, B., Ciotti, M., et al., & Bagni, C. (2012). BC1-FMRP interaction is modulated by 2′-O-methylation: RNA-binding activity of the tudor domain and translational regulation at synapses. *Nucleic Acids Research*.

Laggerbauer, B., Ostareck, D., Keidel, E. M., Ostareck-Lederer, A., & Fischer, U. (2001). Evidence that fragile X mental retardation protein is a negative regulator of translation. *Human Molecular Genetics, 10*, 329–338.

Lewis, H. A., Musunuru, K., Jensen, K. B., Edo, C., Chen, H., Darnell, R. B., & Burley, S. K. (2000). Sequence-specific RNA binding by a nova KH domain. *Cell, 100*, 323–332.

Lugenbeel, K. A., Peier, A. M., Carson, N. L., Chudley, A. E., & Nelson, D. L. (1995). Intragenic loss of function mutations demonstrate the primary role of FMR1 in fragile X syndrome. *Nature Genetics, 10*, 483–485.

Matunis, M. J., Michael, W. M., & Dreyfuss, G. (1992). Characterization and primary structure of the poly(C)-binding heterogeneous nuclear ribonucleoprotein complex K protein. *Molecular and Cellular Biology, 12*, 164–171.

Mila, M., Castellvi-Bel, S., Sanchez, A., Lazaro, C., Villa, M., & Estivill, X. (1996). Mosaicism for the fragile X syndrome full mutation and deletions within the CGG repeat of the FMR1 gene. *Journal of Medical Genetics, 33*, 338–340.

Miyashiro, K. Y., Beckel-Mitchener, A., Purk, T. P., Becker, K. G., Barret, T., Liu, L., … Eberwine, J. (2003). RNA cargoes associating with FMRP reveal deficits in cellular functioning in Fmr1 null mice. *Neuron, 37*, 417–431.

Muddashetty, R. S., Nalavadi, V. C., Gross, C., Yao, X., Xing, L., Laur, O., … Bassell, G. J. (2011). Reversible Inhibition of PSD-95 mRNA translation by miR-125a, FMRP phosphorylation, and mGluR signaling. *Molecular Cell, 42*, 673–688.

Musco, G., Kharrat, A., Stier, G., Fraternali, F., Gibson, T. J., Nilges, M., & Pastore, A. (1997). The solution structure of the first KH domain of FMR1, the protein responsible for the fragile X syndrome. *Nature Structural Biology, 4*, 712–716.

Napoli, I., Mercaldo, V., Boyl, P. P., Eleuteri, B., Zalfa, F., De Rubeis, S., Di Marino, D., … Bagni, C. (2008). The fragile X syndrome protein represses activity-dependent translation through CYFIP1, a new 4E-BP. *Cell, 134*, 1042–1054.

Oberle, I., Rousseau, F., Heitz, D., Kretz, C., Devys, D., Hanauer, A., … Mandel, J. (1991). Instability of a 550-base pair DNA segment and abnormal methylation in fragile X syndrome. *Science, 252*, 1097–1102.

Parrinello, M., & Rahman, A. (1981). Polymorphic transitions in single-crystals – A new molecular-dynamics method. *Journal of Applied Physics, 52*, 9.

Petek, E., Kroisel, P. M., Schuster, M., Zierler, H., & Wagner, K. (1999). Mosaicism in a fragile X male including a *de novo* deletion in theFMR1 gene. *American Journal of Medical Genetics, 84*, 229–232.

Pozdnyakova, I., & Regan, L. (2005). New insights into Fragile X syndrome. Relating genotype to phenotype at the molecular level. *FEBS, J272*, 872–878.

Ramos, A., Hollingworth, D., Adinolfi, S., Castets, M., Kelly, G., Frenkiel, T. A., … Pastore, A. (2006). The structure of the N-terminal domain of the fragile X mental retardation protein: A platform for protein-protein interaction. *Structure, 14*, 21–31.

Ramos, A., Hollingworth, D., & Pastore, A. (2003a). G-quartet-dependent recognition between the FMRP RGG box and RNA. *RNA, 9*, 1198–1207.

Ramos, A., Hollingworth, D., & Pastore, A. (2003b). The role of a clinically important mutation in the fold and RNA-binding properties of KH motifs. *RNA, 9*, 293–298.

Say, E., Tay, H. G., Zhao, Z. S., Baskaran, Y., Li, R., Lim, L., & Manser, E. (2010). A functional requirement for PAK1 binding to the KH(2) domain of the fragile X protein-related FXR1. *Molecular Cell, 38*, 236–249.

Schaeffer, C., Bardoni, B., Mandel, J. L., Ehresmann, B., Ehresmann, C., & Moine, H. (2001). The fragile X mental retardation protein binds specifically to its mRNA via a purine quartet motif. *EMBO, J20*, 4803–4813.

Siomi, H., Choi, M., Siomi, M. C., Nussbaum, R. L., & Dreyfuss, G. (1994). Essential role for KH domains in RNA binding: Impaired RNA binding by a mutation in the KH domain of FMR1 that causes fragile X syndrome. *Cell, 77*, 33–39.

Siomi, M. C., Zhang, Y., Siomi, H., & Dreyfuss, G. (1996). Specific sequences in the fragile X syndrome protein FMR1 and the FXR proteins mediate their binding to 60S ribosomal subunits and the interactions among them. *Molecular and Cellular Biology, 16*, 3825–3832.

Sjekloća, L., Konarev, P. V., Eccleston, J., Taylor, I. A., Svergun, D. I., & Pastore, A. (2009). A study of the ultrastructure of fragile-X-related proteins. *Biochemical Journal, 419*, 347–357.

Tamanini, F., Van Unen, L., Bakker, C., Sacchi, N., Galjaard, H., Oostra, B. A., & Hoogeveen, A.T. (1999). Oligomerization properties of fragile-X mental-retardation protein (FMRP) and the fragile-X-related proteins FXR1P and FXR2P. *Biochemical Journal, 343*, 517–523.

Tarleton, J., Richle, R., Schwarsz, C., Rao, K., Aylsworth, A. S., & Lachlewicz, A. (1993). An extensive *de novo* deletion removing FMR1 in a patient with mental retardation and the fragile X syndrome phenotype. *Human Molecular Genetics, 2*, 1973–1974.

Valverde, R., Edwards, L., & Regan, L. (2008). Structure and function of KH domains. *FEBS, J275*, 2712–2726.

Valverde, R., Pozdnyakova, I., Kajander, T., Venkatraman, J., & Regan, L. (2007). Fragile X mental retardation syndrome: Structure of the KH1-KH2 domains of fragile X mental retardation protein. *Structure, 15*, 1090–1098.

Van Der Spoel, D., Lindahl, E., Hess, B., Groenhof, G., Mark, A. E., & Berendsen, H. J. (2005). GROMACS: Fast, flexible, and free. *Journal of Computational Chemistry, 26*, 1701–1718.

Verkerk, A. J., Pieretti, M., Sutcliffe, J. S., Fu, Y. H., Kuhl, D. P., Pizzuti, A., … Warren, S. T. (1991). Identification of a gene (FMR-1) containing a CGG repeat coincident with a breakpoint cluster region exhibiting length variation in fragile X syndrome. *Cell, 65*, 905–914.

Wang, T., Bray, S. M., & Warren, S. T. (2012). New perspectives on the biology of fragile X syndrome. *Current Opinion in Genetics & Development, 22*, 256–263.

Zalfa, F., Eleuteri, B., Dickson, K. S., Mercaldo, V., De Rubeis, S., di Penta, A., … Bagni, C. (2007). A new function for the fragile X mental retardation protein in regulation of PSD-95 mRNA stability. *Nature Neuroscience, 10*, 578–587.

Zalfa, F., Giorgi, M., Primerano, B., Moro, A., Di Penta, A., Reis, S., … Bagni, C. (2003). The fragile X syndrome protein FMRP associates with BC1 RNA and regulates the translation of specific mRNAs at synapses. *Cell, 112*, 317–327.

Zhang, Y., O'Connor, J. P., Siomi, M. C., Srinivasan, S., Dutra, A., Nussbaum, R. L., et al. (1995). The fragile X mental retardation syndrome protein interacts with novel homologs FXR1 and FXR2. *EMBO J.14*: 5358–5366.